PHYSICAL REVIEW B **81**, 165437 (2010)

Coherent hard x-ray diffractive imaging of nonisolated objects confined by an aperture

Sunam Kim, Chan Kim, Suyong Lee, Shashidhara Marathe, and D. Y. Noh*
Department of Materials Science and Engineering & Nanobio Materials and Electronics, Graduate Program of Photonics and Applied Physics, Gwangju Institute of Science and Technology, Gwangju 500-712, Korea

H. C. Kang
Department of Advanced Materials Engineering and BK21 Education Center of Mould Technology for Advanced Materials and Parts, Chosun University, Gwangju 501-759, Korea

S. S. Kim, A. Sandy, and S. Narayanan
Advanced Photon Source, Argonne National Laboratory, Argonne, Illinois 60439, USA
(Received 27 March 2010; published 27 April 2010)

Coherent hard x-ray imaging of nonisolated weak phase objects is demonstrated by confining x-ray beam in a region of a few micrometers in cross section using a micrometer-sized aperture. Two major obstacles in the hard x-ray coherent diffraction imaging, isolating samples and obtaining central speckles, are addressed by using the aperture. The usefulness of the proposed method is illustrated by reconstructing the exit wave field of a nanoscale trench structure fabricated on silicon which serves as a weak phase object. The quantitative phase information of the exit wave field was used to reconstruct the depth profile of the trench structure. The scanning capability of this method was also briefly discussed.

DOI: 10.1103/PhysRevB.81.165437 PACS number(s): 07.85.Tt, 42.30.Rx, 61.05.cf, 81.70.Tx

I. INTRODUCTION

Coherent diffraction imaging (CDI) has emerged as a promising nanoscale probe since it provides not only the shape but also quantitative internal structure of a nanoscale object with a spatial resolution limited only by the wavelength of probing light.[1] It retrieves an image from an oversampled diffraction signal without employing any lenses using computational algorithms.[2–4] CDI based on hard x rays of wavelength below 2 Å is especially attractive due to the excellent spatial resolution provided by extremely short wavelength. The main advantage of the hard x-ray CDI, however, lies in that internal structure of a specimen could be explored under nonvacuum *in situ* environments.[5] This forte enlarges the application area of the CDI greatly.

To retrieve the lost phase information in diffraction signal, the oversampling methods impose that the sampling size be at least twice the object size in real space.[6] Typically, this requirement in the hard x-ray CDI has been addressed by isolating micrometer or submicrometer size specimen in surrounding no density area.[7,8] Isolating specimens, however, is difficult or unachievable under many physical and chemical environments, which limits the application of the hard x-ray CDI greatly. Contamination of scattering signal in low momentum-transfer Q region imposes another major difficulty in the hard x-ray CDI. Strong direct beam together with the parasitic scattering generated by the slits defining x-ray beam in a cross-sectional area of a few tens of micrometer in size makes it practically impossible to measure central speckles near the forward zeroth-order diffraction peak.[9,10] Despite their significance in the image reconstruction, central speckles had to be filtered out in previous CDI reports and replaced by simulated data based on low resolution microscopy images[1,3,11,12] or with calculated data from computational methods.[7,13] Replacing the missing speckles from secondary data was successful in some cases but this is not always applicable.

On the other hand, in CDI reports using optical and soft x-ray lasers, the oversampling requirement has mostly been achieved by confining the illumination area of objects by blocking light using an aperture.[14–16] Although this method is of great advantage in imaging continuous natural objects, it has not been often adopted in hard x-ray CDI due to the difficulties in the fabrication of the hard x-ray beam defining optics. To block highly penetrating hard x ray effectively, an aperture with an opening of a few micrometers in size should have a thickness of order 100 μm, much larger than the opening size.

Several technical achievements on the illumination confinement in hard x-ray CDI for extended objects were recently reported.[17,18] Rodenburg *et al.*[19] achieved the oversampling condition by blocking beam with a micropinhole and proposed a method based on ptychography for extended objects. Abbey *et al.* reported a keyhole coherent diffraction imaging technique where focused x-ray beam by a Fresnel zone plate was used. Although these works expanded the potential application area of hard x-ray CDI greatly, the demonstrations have typically been limited to relatively strong phase object due to significant amount of parasitic scattering from beam defining optics. This limits the application to weak phase objects such as biospecimens greatly. It was also difficult to extract quantitative information of an object other than its image. Up to now, pinholes are punched on a metal piece by an intense laser beam or focused ion beam, which have rather poor edges due to the melt contaminants. High aspect ratio imposes another difficulty. Therefore, developing improved beam confining optics is essential in improving reconstructed image quality.

In this paper, we report an application of a micrometer sized rectangular aperture composed of four polished tantalum blades to the hard x-ray CDI. The two major challenges discussed above are addressed by the application of the aperture. The wave field of the x-ray beam at the exit plane of

 ©2010 The American Physical Society

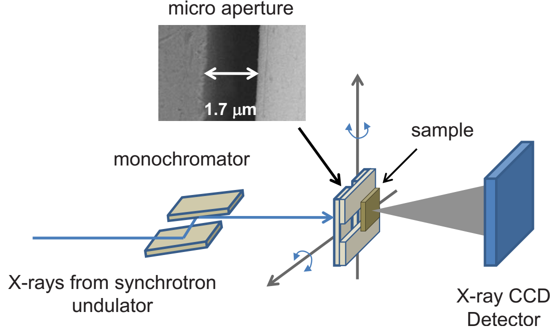

FIG. 1. (Color online) Schematic diagram of the CDI experimental setup using micrometer sized aperture. The x-ray beam is confined by a micrometer size aperture made of polished tantalum blades.

an object was retrieved using an oversampling algorithm. Furthermore, an application of the pinhole to image a weak phase object is given in order to demonstrate its usefulness. We also demonstrated the scanning capability of the proposed method.

The wave field of the x-ray beam propagating along the z direction through an object confined by an aperture opening A is given by

$$\psi(x,y) = \begin{cases} \psi_0(x,y)\exp\left(ik\int_{z_i(x,y)}^{z_f(x,y)} n_c dz\right), & \text{if } (x,y) \in A \\ 0, & \text{otherwise}, \end{cases} \tag{1}$$

where $\psi_0(x,y)$ is the incident plane wave field, k is the x-ray wave vector $2\pi/\lambda$, $n_c(x,y,z)$ is the complex index of refraction which is represented by $1-\delta+i\beta$ in x-ray regime, and $z_i(z_f)$ is the start (end) position of the specimen along the x-ray propagation direction at a lateral position (x,y). The real part δ of the index of refraction is related to the atomic density ρ_a of the object by $\delta=2\pi\rho_a f_r r_0/k^2$, where r_0 is the classical radius of electron and f_r is the real part of atomic form factor.[20] The imaginary part β is responsible for the absorption and typically much smaller than δ. The aperture opening A defines the support area required in the oversampling method outside which the wave field is zero. The wave field thus provides the electron-density map integrated along the propagation direction as a function of the lateral coordinates.

II. EXPERIMENTAL CONFIGURATIONS

Figure 1 shows the hard x-ray CDI configuration employed in this experiment schematically. The experiment was performed at an undulator beamline 11A at Pohang Light Source (PLS) and at the beamline at 8 ID at Advanced Photon Source (APS). Most of the data presented here were obtained at PLS with the x-ray energy fixed to 5.5 keV ($\lambda=2.25$ Å) by a polished Si(111) double bounce monochromator. A harmonic rejection mirror was used at APS while no mirror was employed at PLS. The flux of x rays at $\lambda/3$ were negligible due to the low electron-beam energy at 2.5 GeV at PLS.

The aperture was an assembly of four polished tantalum blades. The surface of the blades was polished mechanically using diamond pastes in steps down to 0.05 μm. A pair of blades was put vertically with a gap close to one micrometer and another pair was put horizontally on top. The resulting assembly had an opening of 1.7 μm$\times$2.2 μm in cross section as estimated by the x-ray diffraction profile. The quality of the blade edges were inspected by taking scanning electron microscopy (SEM) as shown in Fig. 1. The final evaluation of the blade quality, however, was done by measuring the x-ray diffraction pattern and comparing it with the simulated pattern from an ideal rectangular aperture. The thickness of the Ta blades was about 130 μm, which attenuates x rays at 5.5 keV by a factor of about 10^{-40} essentially completely. We note that x-ray beam had to travel through a long tunnel because the aspect ratio was 100. It was, therefore, crucial to align the aperture using two rotational and translational motions.

Samples can be attached at the downstream of a rectangular aperture or placed on a translational stage for the purpose of scanning. The diffraction pattern from a sample were captured by a deep-depletion direct illumination charge-coupled-device (CCD) detector (Princeton Instrument, pixel size, 20 μm$\times$20 μm) placed at about 1440 mm downstream of the sample. Considering the whole opening of the aperture as unknown sample support area, the oversampling ratio, the ratio of the sampling area given by the reciprocal of the pixel resolution in Q space, to the sample support area was about 70.[21] A beamstop was employed to block the intense central scattering signal to record the weak speckles at high diffraction angles. The central speckles were measured independently by attenuating the signal using a double-side polished silicon wafer in front of the CCD detector with the beamstop removed. The thickness of the wafer was 100 ± 5 μm with the roughness of order few 10 nm. The effect of the attenuator silicon on the diffraction profile was investigated and no significant change in the diffraction intensity profile other than the overall attenuation was observed. To overcome the limited dynamic range of the CCD and to increase the signal-to-noise ratio, 1000 frames are averaged to form a diffraction pattern.

III. RESULTS AND DISCUSSIONS

A. Reconstruction of empty pinhole

The wave field of the x-ray beam at the exit plane of the aperture was reconstructed from a far-field diffraction pattern shown in Fig. 2(a). Diffraction features of a rectangular aperture close to an ideal one are illustrated in the figure. High-order speckles are much more pronounced than those from a roller blade type slit reported previously.[22] A line profile along the vertical Q_y direction measured at $Q_x=0$ shown in Fig. 2(b) illustrates that the measured diffraction pattern matches well with theoretical intensity profile of a rectangular aperture. The simulated intensity profile shown in a solid line is an ideal squared sinc function blurred only by CCD pixel resolution function. We emphasize that the central speckles including the zeroth and the first order were recorded clearly. The diffraction signal up to the momentum

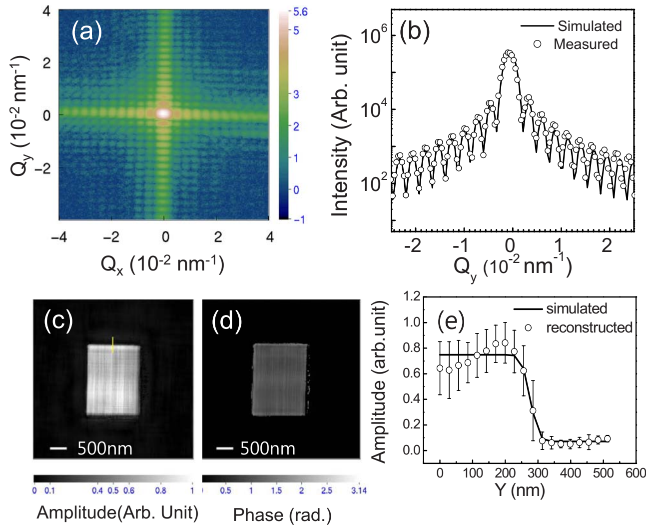

FIG. 2. (Color online) (a) Coherent diffraction amplitude of the rectangular aperture assembly. (b) Diffraction profile along the vertical direction with the horizontal position fixed at the center. The solid line is the simulation of an ideal aperture. (c) Amplitude of the reconstructed wave field at the exit of the aperture. (d) Reconstructed phase map of the exit wave field. (e) Line profile of the reconstructed amplitude across the edge indicated in (c). The solid line is a fit to an error function.

transfer of 0.115 nm^{-1} was used as the modulus of the far-field wave field, which defines the numerical aperture and the image resolution.

The Shrinkwrap algorithm based on the hybrid-input-output (HIO) algorithm[2] was adopted to reconstruct the phase and the amplitude of the x-ray wave field at the exit plane of the aperture.[23] In a typical HIO algorithm, the experimentally determined diffraction amplitude together with an initial trial phase is Fourier transformed to get a real-space wave field. A support constraint, typically imposing zero density outside a known support, is applied to the wave field and the resulting wave field is inverse Fourier transformed to reciprocal space. The phase thus obtained together with the experimental diffraction amplitude was used in the subsequent iteration. The Shrinkwrap algorithm, however, estimates the support from the autocorrelation function, the inverse Fourier transform of diffraction intensity which is twice the size of the object. This support gets updated as the iterations proceed and approaches the true object. In our reconstruction routine, the support was updated at every 20th iteration by thresholding the real-space wave field amplitude at 10% of its maximum after blurring its boundary multiplying a Gaussian blurring function. This provided a support mask tightly tracing the boundary of the object as the number of iterations increased. An error estimate in real space, E_s^2 defined as

$$E_s^2 = \frac{\sum_{x,y \notin s} |\psi_n(x,y)|^2}{\sum_{x,y \in s} |\psi_n(x,y)|^2}, \tag{2}$$

where ψ_n is reconstructed wave field at nth iteration and s is the support area, was used as indicator of the convergence of the iteration. Once E_s^2 reached 10^{-4}, the algorithm was stopped after additional 500 iterations.

The reconstructed phase and the amplitude of the exit wave field are shown in Figs. 2(c) and 2(d), respectively. The results are the average of 12 reconstructions each starting with a random initial values.[8,24] Each individual reconstruction was obtained in about 1000 iterations. The overall phase of each reconstructed wave field was adjusted by adding a constant phase factor prior to the averaging. The amplitude of the reconstructed image exhibits a rectangular pinhole of 1.7 μm $\times$ 2.2 μm. The optimum spatial resolution estimated by the size of the numerical aperture was 27 nm. This corresponds to a single pixel size in the reconstructed image. Consistently, the width of an error function describing the line profile of the wave amplitude across the edge of the aperture indicated in Fig. 2(e) was about 22 nm. The variation in the phase of the exit wave field shown in Fig. 2(d) was about 0.07 radians. We attribute the fluctuations in the phase value to the noises from the parasitic scattering of the pinhole and the data recording process, although we cannot completely rule out possible unknown causes in the reconstruction algorithm.

B. Reconstruction of nonisolated objects attached to an aperture

In order to investigate the applicability of the proposed hard x-ray CDI using a microaperture, we attached a nonisolated weak phase object, a one-dimensional trench structure fabricated on a Si substrate, to the aperture. The SEM images showing the top and side views of the trench structure are shown in Fig. 3(a). The height of the trench was about 680 nm and the lateral trench period d was about 380 nm. The diffraction pattern of the trench structure shown in Fig. 3(b) was obtained following the procedure discussed in the experimental section. It represents a convolution function of the diffraction pattern of a rectangular aperture and the complex transmittance function of the specimen. Series of bright Bragg spots appear at $Q=2n\pi/p$ (n is an integer number and p is the period of the trench structure) along the diagonal direction which originates from the periodic trench structure. The spots are decorated by the 2D sinc function of the rectangular aperture.

The reconstruction of the exit wave field right after the trench structure was also performed using the Shrinkwrap algorithm treating the wave field as a complex quantity. In this case, diffraction signals up to 0.17 nm^{-1} were used as the Fourier modulus constraint. Ideally, the aperture function shown in Fig. 2(c) obtained previously can be utilized as a fixed support for the reconstruction. In this work, however, the support deduced by the Shrinkwrap algorithm directly from the diffraction pattern served better due to the slight change in the aperture configuration during the process of the sample attachment. Figures 3(c) and 3(d) show the amplitude and the phase of the reconstructed exit wave field which are the average of 11 consistent individual reconstructions each obtained by 1000 iterations. The support area corresponds to about 100 $\times$ 128 pixels. The amplitude shown in Fig. 3(c) displays a rather weak contrast due to the negligible absorp-

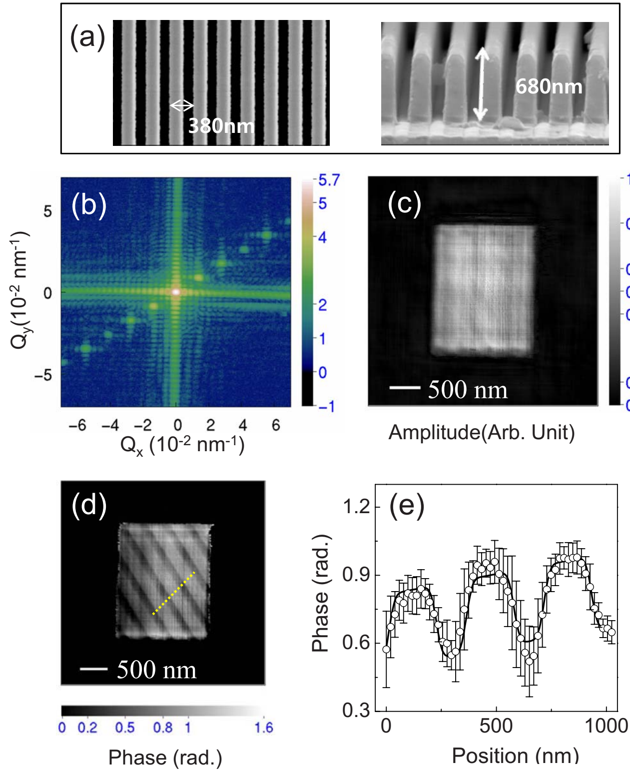

FIG. 3. (Color online) (a) Top and side view of an SEM image of the trench structure. (b) Diffraction pattern of the trench structure defined by the rectangular aperture. [(c) and (d)] Amplitude (c) and phase (d) of the reconstructed exit wave field. (e) Line profile of the phase map. The solid line is a fit to a trench structure assuming the image resolution of 48 nm.

tion contrast. The absorption coefficient β for silicon at 5.5 keV is about 7.6×10^{-7}, and the difference in the attenuation factor at the top and bottom of the trench is only about 1%. Different from the amplitude image, however, the reconstructed phase map shown in Fig. 3(d) exhibits the image of the periodic trench structure clearly.

One of the major advantages of the hard x-ray CDI is that it provides not only the image of a specimen but also the projected electron density as function of the lateral position quantitatively. From Eq. (1), the wave field at the exit of the trench structure can be approximated as $\psi_0 e^{i\phi_0}e^{ik\delta t(x,y)}$, where $t(x,y)$ is the thickness of the silicon at a position (x,y). We have assumed that the incident wave was a plane wave. One may calculate the depth d of the trench from the difference between the phase value at the top and at the bottom of the trench. The phase difference $\Delta\phi$ is given by $k\delta(t_{top}-t_{bottom})$, where $t_{top}-t_{bottom}$ corresponds to the depth of the trench d. A line profile of the phase image is illustrated in Fig. 3(e). We think that the overall slope is due to the variation in the total thickness of the silicon substrate. The lateral resolution of the trench specimen is increased as compared to the bare aperture even with the increased numerical aperture due to the decrease in the intensity between the Bragg spots. The diffraction intensity up to the eighth-order Bragg spot was reliably usable, which sets up the lateral resolution of about 48 nm. By fitting the line profile to a trench structure convoluted by the image resolution of 48 nm, we obtain $\Delta\phi$ of 0.37 ± 0.06 rad. This corresponds to the trench depth $d=800\pm130$ nm when we employ the reported value of $\delta=1.63\times10^{-5}$ of silicon. This depth thus obtained is larger than the value estimated from the SEM image but with the error. We note that the estimation of the depth profile from the phase map is only possible when one may assume that the density of an object is uniform. In general, the phase contrast corresponds to the electron density projected along the direction of the x-ray propagation as explained in Eq. (1).

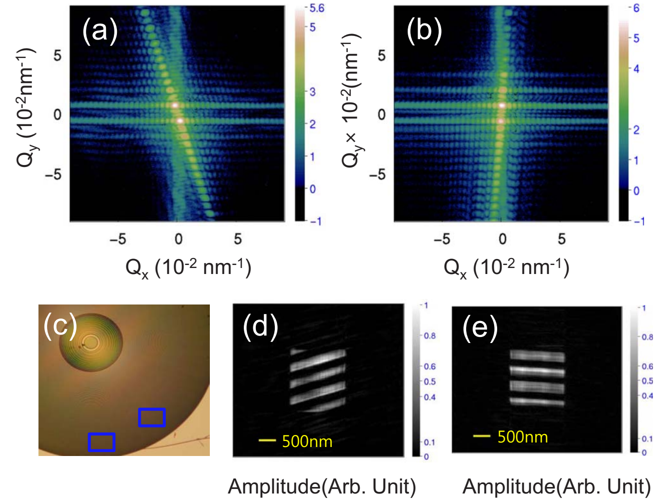

FIG. 4. (Color online) [(a) and (b)] Far field diffraction patterns of the parts of a Fresnel zone plate indicated in (c). The diffraction patterns were recorded at 5.5 keV X-ray energy and displayed in logarithmic map. (c) Optical micrograph of the zone plate used as a test object. [(d) and (e)] Reconstructed images corresponding to diffraction pattern shown in (a) and (b), respectively.

Accurate determination of the phase value quantitatively has been difficult for hard x-ray CDI based on the illumination confinement. Although the resulting images reconstructed by the iteration algorithm starting from different initial phases are qualitatively similar, the fluctuation in the quantitative phase value is not negligible. The major source of the difficulty lies in the noise signal in the process of the beam confinement. Therefore, objects with a phase contrast close to 2 rad, such as thick metal pattern on silicon, have been used to demonstrate the imaging capability of the hard x-ray CDI using illumination confinement.[19] The phase contrast of the trench structure reported in this work, 0.32 rad, is much smaller than other systems reported up to now. The error bar, accuracy of the phase value, 0.06 rad, is significantly improved. For typical biospecimens, we estimate that the phase contrast is below 0.1 rad and further improvement is required by reducing the noise signals from the aperture and enhancing the coherency of the x-ray beam.

Applicability of the aperture based hard x-ray CDI to a truly extended object was examined by placing a test object at about 100 μm downstream of the aperture without attaching directly to the aperture. At this position, the Fresnel number was about 180 and one may approximate the incident wave field as a plane-wave field truncated by the aperture without worrying about the effect of propagation. A Fresnel zone plate with a diameter of 580 μm made of silicon was used as the test object. The height difference between the

thick and thin part of a zone was around 9 μm. When the x rays are transmitted, the expected phase difference is about 4 rad. The zone plate was mounted on a two-dimensional linear stage which allowed the scanning of the zone plate. An optical microscope image of the zone plate is displayed in Fig. 4(c). Figures 4(a) and 4(b) show the far-field diffraction pattern recorded at two different regions of the specimen indicated in the microscopic image. Both diffraction patterns are noncentrosymmetric indicating that the transmittance function of the sample is complex as expected. Different from the diffraction pattern of the silicon trench structure which is a weak phase object, the central part of the diffraction pattern is modified greatly. We note that the second-order speckles became stronger than the zeroth-order speckle. The amplitudes of the reconstructed exit wave are shown in Figs. 4(d) and 4(e).

IV. CONCLUSION

In summary, we have demonstrated a hard x-ray CDI of nonisolated objects using a micrometer-sized rectangular aperture. The x-ray wave field at the exit of the empty aperture was reconstructed using the oversampling method. In addition, the amplitude and the phase of the exit wave field through a trench structure on silicon were reconstructed. The image of the trench structure was well illustrated in the resulting phase map. The depth profile of the trench was obtained from the phase difference between the top and bottom of the trench. Through this work, we have addressed the two major issues in the hard x-ray coherent diffraction imaging, isolating samples and obtaining central speckles, by using a hard x-ray aperture. We believe that this work enlarge the applicability of the hard x-ray CDI to nonisolated weak phase objects.

ACKNOWLEDGMENTS

This work was supported by the Korean National Research Foundation (NRF) through the NCRC (Grant No. R15-2008-006-00000-0) and WCU (Grant No. R31-2008-10026-0). We acknowledge the support from GIST Photonics 2020 Project and the Ultrashort Quantum Beam Facility Program of the Korean Ministry of Knowledge and Economy. Use of the Advanced Photon Source was supported by the U.S. Department of Energy under Contract No. DE-AC02-06CH11357.

*dynoh@gist.ac.kr

[1] J. Miao, P. Charalambous, J. Kirz, and D. Sayre, Nature (London) **400**, 342 (1999).
[2] J. R. Fienup, Opt. Lett. **3**, 27 (1978).
[3] J. Miao, T. Ishikawa, E. H. Anderson, and K. O. Hodgson, Phys. Rev. B **67**, 174104 (2003).
[4] J. Miao, K. O. Hodgson, and D. Sayre, Proc. Natl. Acad. Sci. U.S.A. **98**, 6641 (2001).
[5] M. A. Pfeifer, G. J. Williams, I. A. Vartanyants, R. Harder, and I. K. Robinson, Nature (London) **442**, 63 (2006).
[6] C. E. Shannon, Proc. IRE **37**, 10 (1949).
[7] J. Miao, C. C. Chen, C. Song, Y. Nishino, Y. Kohmura, T. Ishikawa, D. Ramunno- Johnson, T. K. Lee, and S. H. Risbud, Phys. Rev. Lett. **97**, 215503 (2006).
[8] Y. Nishino, Y. Takahashi, N. Imamoto, T. Ishikawa, and K. Maeshima, Phys. Rev. Lett. **102**, 018101 (2009).
[9] F. van der Veen and F. Pfeiffer, J. Phys.: Condens. Matter **16**, 5003 (2004).
[10] K. J. Gaffney and H. N. Chapman, Science **316**, 1444 (2007).
[11] J. Miao, K. O. Hodgson, T. Ishikawa, C. A. Larabell, M. A. LeGros, and Y. Nishino, Proc. Natl. Acad. Sci. U.S.A. **100**, 110 (2003).
[12] J. Miao, J. E. Amonette, Y. Nishino, T. Ishikawa, and K. O. Hodgson, Phys. Rev. B **68**, 012201 (2003).
[13] Y. Nishino, J. Miao, and T. Ishikawa, Phys. Rev. B **68**, 220101(R) (2003).
[14] J. C. H. Spence, U. Weierstall, and M. Howells, Philos. Trans. R. Soc. London, Ser. A **360**, 875 (2002).
[15] H. N. Chapman, A. Barty, M. J. Bogan, S. Boutet, M. Frank, S. P. Hau-Riege, S. Marchesini, B. W. Woods, S. Bajt, W. Henry Benner, R. A. London, E. Plönjes, M. Kuhlmann, R. Treusch, S. Düsterer, T. Tschentscher, J. R. Schneider, E. Spiller, T. Möller, C. Bostedt, M. Hoener, D. A. Shapiro, K. O. Hodgson, D. van der Spoel, F. Burmeister, M. Bergh, C. Caleman, G. Huldt, M. Marvin Seibert, F. R. N. C. Maia, R. W. Lee, A. Szöke, N. Timneanu, and J. Hajdu, Nat. Phys. **2**, 839 (2006).
[16] R. L. Sandberg, A. Paul, D. A. Raymondson, S. Hadrich, D. M. Gaudiosi, J. Holtsnider, R. I. Tobey, O. Cohen, M. M. Murnane, H. C. Kapteyn, C. Song, J. Miao, Y. Liu, and F. Salmassi, Phys. Rev. Lett. **99**, 098103 (2007).
[17] P. Thibault, M. Dierolf, A. Menzel, O. Bunk, C. David, and F. Pfeiffer, Science **321**, 379 (2008).
[18] B. Abbey, K. A. Nugent, G. J. Williams, J. N. Clark, A. G. Peele, M. A. Pfeifer, M. De Jonge, and I. McNulty, Nat. Phys. **4**, 394 (2008).
[19] J. M. Rodenburg, A. C. Hurst, A. G. Cullis, B. R. Dobson, F. Pfeiffer, O. Bunk, C. David, K. Jefimovs, and I. Johnson, Phys. Rev. Lett. **98**, 034801 (2007).
[20] J. Als-Nielsen and D. McMorrow, *Element of Modern X-ray Physics* (Wiley, West Sussex, England, 2001), Chap. 3.
[21] J. Miao and D. Sayre, Acta Crystallogr., Sect. A: Found. Crystallogr. **56**, 596 (2000).
[22] D. Le Bolloc'h, F. Livet, F. Bley, T. Schulli, M. Veron, and T. H. Metzger, J. Synchrotron Radiat. **9**, 258 (2002).
[23] S. Marchesini, H. He, H. N. Chapman, S. P. Hau-Riege, A. Noy, M. R. Howells, U. Weierstall, J. C. H. Spence, Phys. Rev. B **68**, 140101(R) (2003).
[24] H. N. Chapman, A. Barty, S. Marchesini, A. Noy, S. P. Hau-Riege, C. Cui, M. R. Howells, R. Rosen, H. He, J. C. H. Spence, U. Weierstall, T. Beetz, C. Jacobsen, and D. Shapiro, J. Opt. Soc. Am. A Opt. Image Sci. Vis **23**, 1179 (2006).